SI Materials and Methods

Sample preparation and single-molecule experiments. The expression, purification, labeling, and bulk turnover measurements of TbQSOX and its variants were performed as previously described (1). Unless otherwise stated, all single-molecule experiments were conducted in 20 mM sodium phosphate, pH 7.5, 200 mM NaCl, 0.01 % Tween 20. The experiments were performed on a MicroTime 200 (PicoQuant, Germany) with two or four detection channels (SPAD, Excelitas) equipped with an Olympus UplanApo 60x/1.20W objective. The donor was excited using a diode laser (LDH-D-C-485, PicoQuant, Germany) either continuously for recurrence experiments or in pulsed mode (40 MHz) for determinations of the fluorescence lifetime of the donor AlexaFluor 488. After passing through a 100 µm pinhole, sample fluorescence was separated into donor and acceptor components using a dichroic mirror (585DCXR, Chroma, Rockingham, VT). After passing two additional filters (Chroma ET525/50M, HQ650/100), each component was focused onto an avalanche photodiode (SPCM-AQR-15, Excelitas, Canada), and the arrival time of every detected photon was recorded using a Hydra Harp counting card (PicoQuant, Berlin, Germany). For fluorescence anisotropy experiments, the emission light was first separated into its components parallel and perpendicular with respect to the linearly polarized excitation light. All measurements were performed with laser powers of 50 µW or 100 µW and for the recurrence experiments, photons were recorded for 10 – 48 hours. In experiments with the substrate DTT, the sample was replaced every 0.5 – 1.5 hours to ensure an excess of substrate and oxygen throughout the experiment and to prevent the oxidation of the dyes by the catalytic product hydrogen peroxide.
Bifunctional poly-ethylene glycol (HS-PEG5000-SH) from JenKem was labeled site specifically with AlexaFluor488 (C_5) maleimide and AlexaFluor488 (C_5) maleimide and subsequently purified using C_{18} reversed phase chromatography.

Identification of molecules. For the identification of photon bins, photons within a time interval of 0.1 ms were combined into one bin, with n_D and n_A photons counted in the donor and acceptor detection channels, respectively. These numbers were corrected for background, differences in quantum yields of donor and acceptor, the different collection efficiencies in the detection channels, cross-talk, and direct acceptor excitation as described previously (2). Transfer efficiency histograms were obtained from bins with $n'_A + n_D > 30$ for RASP and from bursts with $n'_A + n_D > 100$ for the analysis of fluorescence lifetimes, widths, and anisotropies. The transfer efficiency is given by:

$$E = \frac{n'_A}{n'_A + \gamma n_D} \qquad (1)$$

with

$$n'_A = n_A - \frac{\alpha}{1+\alpha}\left(n_A + \gamma n_D\right) - \beta n_D .$$

Where $\alpha = 0.048$ is the ratio of the extinction coefficients of Alexa 594 and Alexa 488 at the laser donor excitation wavelength ($\lambda_{ex,D} = 485$ nm), β is the fraction of donor photons detected in the acceptor channel (crosstalk), and $\gamma = \eta_A Q_A / \eta_D Q_D$ is the ratio of the products of quantum yields and detection efficiencies for acceptor and donor. The values for α, β, and γ at room temperature ($T = 296$ K) were determined as described previously (2). The shot noise limited width of the FRET histogram in Fig. 1c was determined by recoloring the original photon trace while keeping the photon arrival times fixed.

Extracting kinetics with RASP. The recurrence analysis of single particles (RASP) uses the fact that a freely diffusing molecule can be observed multiple times in a single-molecule experiment (Fig. 1D, main text). Once a molecule leaves the observation volume, the chance to return to the confocal spot is greater than the chance of detecting a new molecule for short time intervals. This effect can be used to extract the kinetics of forming the 'open' state from molecules in the 'closed' state and *vice versa*. To extract the kinetics, we first identify all bins with transfer efficiencies indicative of the closed state ($E \geq 0.8$). In a second step, we construct FRET-histograms for those bins that follow the originally identified set in the window $\left(t-T,t\right)$, with t being the time shift. With increasing t, the relative population of closed molecules decays in the recurrence histograms while the population of open molecules increases (Fig. S1A). Two factors contribute to this redistribution: (*i*) the conformational dynamics of TbQSOX, i.e., molecules that were initially in the 'closed' state switch to the 'open' state at longer times, and (*ii*) the arrival of new molecules in the observation volume.

To disentangle the two contributions, we determine $p_{same}\left(t\right)$, which is the probability that two bins at time t_1 and t_2 (with $t = t_2 - t_1$) result from the same molecule (Fig. S1B). This quantity is directly accessible from the bin-pair autocorrelation functions (3) and characterizes the frequency with which new molecules enter the confocal volume. The bin-pair autocorrelation function is defined as

$$g\left(t\right) = \frac{p\left(\left\{b_1,t_1\right\},\left\{b_2,t_1+t\right\}\right)}{p\left(\left\{b_1,t_1\right\},\left\{b_2,t_1\right\}\right)} . \qquad (2)$$

Here, $p(\{b_1, t_1\},\{b_2, t_1+t\})$ denotes the joint probability of observing two bins b_1 and b_2 at times t_1 and t_1+t, respectively and $p(\{b_1, t_1\})$ and $p(\{b_2, t_1\})$ are the probabilities of detecting bin b_1 and b_2, respectively, at time t_1 (3). Thus, eq. 2 provides the

timescale up to which the occurrence of successive bins is correlated and it directly relates to the probability that two successive bins b_1 and b_2 are from the same molecule, which is given by

$$p_{same}(t) = 1 - \frac{1}{g(t)}. \quad (3)$$

The knowledge of $p_{same}(t)$ (Fig. S1B) can now be used to compute the RASP-kinetics in the absence of conformational exchange, i.e., for heterogeneity that is static on the recurrence timescale of 100 μs – 20 ms in our case. The observed increase in the population of 'open' molecules in the recurrence histograms after selecting 'closed' molecules initially, $p_{obs}(t)$, is then given by

$$p_{obs}(t) = p_{same}(t)\,p_{conf}(t) + \left[1 - p_{same}(t)\right]\rho. \quad (4)$$

Here, $p_{conf}(t)$ is the kinetics of forming the open state due to conformational dynamics and ρ is the equilibrium fraction of 'open' molecules, which is accessible from the measured FRET-histogram (Fig. 1B). In the absence of conformational dynamics, i.e., for $p_{conf}(t) \to 0$, equation 4 reduces to

$$p_{obs}(t) = \left[1 - p_{same}(t)\right]\rho, \quad (5)$$

which provides the kinetics in the sole presence of static heterogeneity. In the presence of conformational exchange however, the term $p_{conf}(t)$ is given by

$$p_{conf}(t) = 1 \Big/ \left[1 - \varepsilon\left(p_o(t)^{-1} - 1\right)\right] \quad (6)$$

with $p_o(t) = 1 - p_c(t)$ being the time-dependent fraction of open molecules that arise due to conformational transitions from the closed state (3) and $p_c(t)$ being the time-dependent fraction of closed molecules shown in the main text (Fig. 2A & 4A). The factor $\varepsilon = \left(\rho_m^{-1} - 1\right) \Big/ \left(\rho^{-1} - 1\right)$ takes potential differences in the molecular brightness of the fluorophores into account. Here, ρ_m and ρ are the measured and correct equilibrium fraction of open molecules, respectively. The recurrence FRET-histograms were fitted with a sum of two log-normal functions to describe the population of closed molecules (high FRET) and molecules that lack an active acceptor dye (E = -0.05), and a Gaussian distribution for open molecules (E = 0.25). The relative populations of open and closed molecules were obtained by integrating the respective sub-populations. To check for potential differences in brightness of the two dyes between the high and low FRET population, we varied the identification

threshold for bins (N_T) from 25 to 50 photons, determined the relative population of closed molecules, and linearly extrapolated this fraction to a threshold of $N_T > 0$. For wt TbQSOX, the relative population of closed molecules is $\rho_m^{\,C} = 8\%$ for $N_T > 30$. The extrapolated value to $N_T > 0$ is $\rho^C = 12\%$, which leads to a correction factor of $\sigma = \rho^C/\rho_m^{\,C} = 1.5$. Thus, the corrected steady-state fraction of open molecules $\rho = \rho^O$ is given by $\rho = 1 - \sigma\left(1 - \rho_m\right)$ with the subscript m indicating the uncorrected fraction of open molecules. To keep the nomenclature of equation 6, we have $\sigma = \left(1 - \rho_m\left(1 + \varepsilon\right)\right)^{-1}$ or $\varepsilon = \left[1 + \sigma\left(\rho_m - 1\right)\right]\big/\rho_m\sigma$ and with eq. 4, the corrected kinetics is given by

$$p_o(t) = \left(\frac{p_{same}(t)}{\varepsilon\left(p_{obs}(t) - \left(1 - p_{same}(t)\right)\rho\right)} - \frac{1}{\varepsilon} + 1 \right)^{-1} \qquad (7)$$

In our case, $\varepsilon = 0.64$. Notably, even though the absolute value of the rate of the decays will depend on the precise values of ε, and hence on the value of σ, the shape of the decay will not (Fig. S4). Thus, the power law behavior is robust with respect to the specific ε-value.

The model-dependent analysis of the kinetics. The solutions of the three-state models shown in the main text are obtained by solving the rate equations $\dot{\mathbf{p}}$=**Kp** , with **p** representing the normalized vector of the three states. The solution was obtained with Mathematica (Version 10.3) and is given in general form by

$$\mathbf{p}(t) = e^{\mathbf{K}t}\mathbf{p_0}\,. \qquad (8)$$

Here, $\mathbf{p}_0$ is the initial distribution of the three states.

The sum of the two open states was used in a fit of the experimental data (Fig. 2A). For the fit, each data point was weighted by the corresponding value of $p_{same}(t)$ to account for the increasing uncertainty of the data at long delay times. The same weighting has also been used for fits with equations 2 and 3 in the main text. Since equation 2 (main text) does not directly provide a rate of the decay, we computed rates as the inverse half-life of the decays. For comparison, the turnover rates are also shown as inverse half-life (Fig. 5C). The turnover rates were fit using a previously suggested model (1)

$$k = \frac{aS^2 + bS}{cS^2 + dS + f} \qquad (9)$$

Here, S is the substrate concentration and a to f are fitting parameters. All rates shown

in the manuscript are inverse half-life.

Relationship between power law and exponential kinetics. The β-exponent from fits of the experimental data with equation 2 (main text) can be taken as an approximate deviation from exponential kinetics. This can be seen by a Taylor expansion of the exponential function around the value $t = 0$. When truncating after the linear term, one obtains

$$p_c(t) = ae^{-kt} + b \approx a(1+kt)^{-1} + b\,. \tag{10}$$

Here, k is a kinetic rate, and a, b are constants. The third equality results in equation 1 in the main text with $\beta = 1$. Hence, for short times, β-exponents closer to one indicate a smaller deviation from exponential behavior.

Subpopulation-specific fluorescence lifetime distribution analysis. Here, we followed the approach of Hoffmann *et al.* (2007) (4). Bursts assigned to the open subpopulation were selected from the transfer efficiency range $0.2 < E < 0.5$ and photons from these bursts were combined to generate time-correlated single-photon counting (TCSPC) histograms, thus leading to the decays $\tilde{I}_D(t)$ and $\tilde{I}_A(t)$, respectively. TCSPC histograms $b_D(t)$ and $b_A(t)$ from all photons not in bursts were used to compute the background-corrected decays $I_D(t)$ and $I_A(t)$ as

$$I_{D,A}(t) = \tilde{I}_{D,A}(t) - \kappa b_{D,A}(t) \tag{11}$$

with κ = (Total subpopulation burst time)/(Total non-burst time).

The resulting decays were finally fitted globally by the equations

$$I_D(t) = IRF_D * h_D(t - t_0)$$
$$I_A(t) = IRF_A * h_A(t - t_0) \tag{12}$$

where

$$h_D(t) = a_D \int_0^{r_{\max}} P_O(r) e^{-k(r)t}\, dr \tag{13a}$$

$$h_A(t) = a_A \int_0^{r_{\max}} P_O(r) \frac{k(r) - k_D}{k(r) - k_A} \left[e^{-k_A t} - e^{-k(r)t} \right] dr + \gamma h_D(t) + \alpha I_0 k_A e^{-k_A t} \tag{13b}$$

are convolved with the instrumental response functions $IRF_{D,A}$ of the donor and acceptor detection channels, respectively. Here, t_0 denotes the time origin of the

decays, k_A is the intrinsic decay rate of the acceptor, k_D the intrinsic decay rate of the donor determined from the population of donor-only molecules (0.29 ns^{-1}), $k(r) = k_D\left(1+(R_0/r)^6\right)$ with the Foerster distance of $R_0 = 5.4$ nm, γ is the photon leakage from the donor to the acceptor channel (0.051), and α is the probability to directly excite the acceptor with the donor excitation (0.048). The function $P_O(r)$ is given by equation 4 in the main text (also eq. S17 below). Free parameters in the global fit were r_0, σ, k_A, and the two amplitudes a_D and a_A, respectively.

Nanosecond–FCS measurements. Cross-correlation curves between acceptor and donor channels were calculated from the photon arrival times and the data were fit over a time window of 4 μs with

$$g_{DA}(\tau) = 1 + \frac{1}{N}\left(1 - c_{AB}e^{-\frac{|\tau - t_0|}{\tau_{AB}}}\right)\left(1 + c_{CD}e^{-\frac{|\tau - t_0|}{\tau_{CD}}}\right)\left(1 + c_T e^{-\frac{|\tau - t_0|}{\tau_T}}\right) \quad (14)$$

for polyethylene glycol 5000 (PEG-5000) and

$$g_{DA}(\tau) = 1 + \frac{1}{N}\left(1 - c_{AB}e^{-\frac{|\tau - t_0|}{\tau_{AB}}}\right)\left(1 + c_T e^{-\frac{|\tau - t_0|}{\tau_T}}\right) \quad (15)$$

for TbQSOX, with N being the mean number of molecules in the confocal volume. The multiplicative terms describe the contribution to the amplitude and timescale of photon anti-bunching (*AB*), chain dynamics (*CD*), and triplet blinking of the dyes (*T*). For clarity, the data shown in Fig. 2E were normalized after fitting by first subtracting 1 from the data, subsequently multiplying with N, dividing by the triplet term, and finally adding 1.

Calculation of time-dependent diffusion coefficients. The potential $V(r)$ in units of $k_B T$ is then given by

$$V(r) = -\ln\left(Z^{-1}\left(P_O(r) + P_C(r)\right)\right) \quad (16)$$

where Z is a normalization factor (Fig. 4B, main text). Here,

$$P_O(r) = r^2 \exp\left(-\frac{1}{2}\left(\frac{r - r_O}{\sigma_O}\right)^2\right) \quad (17)$$

with r_O = 2.75 nm and σ_O = 3.2 nm. The estimated distance distribution of the closed state is given by

$$P_C(r) = a\exp\left(-\frac{1}{2}\left(\frac{r-r_C}{\sigma_C}\right)^2\right) \tag{18}$$

with r_C = 2.2 nm and the width σ_C = 0.1 nm, and a = 55 to reproduce the equilibrium fraction of 12% closed molecules. We use eq. 16-18 to solve eq. 5 of the main text between the boundary conditions r_1 = 0 nm and r_2 = 15 nm with the initial distribution

$$p(r,0) = Z^{-1}\exp\left(-\frac{1}{2}\left(\frac{r-2.2}{0.05}\right)^2\right). \tag{19}$$

The calculated fraction of closed molecules is finally given by

$$f_{calc}(t) = \int_{r_1}^{r_b} p(r,t)\,dr \Big/ \int_{r_1}^{r_2} p(r,t)\,dr\,. \tag{20}$$

with r_b = 2.54 nm being the position of the barrier top.

Figures.

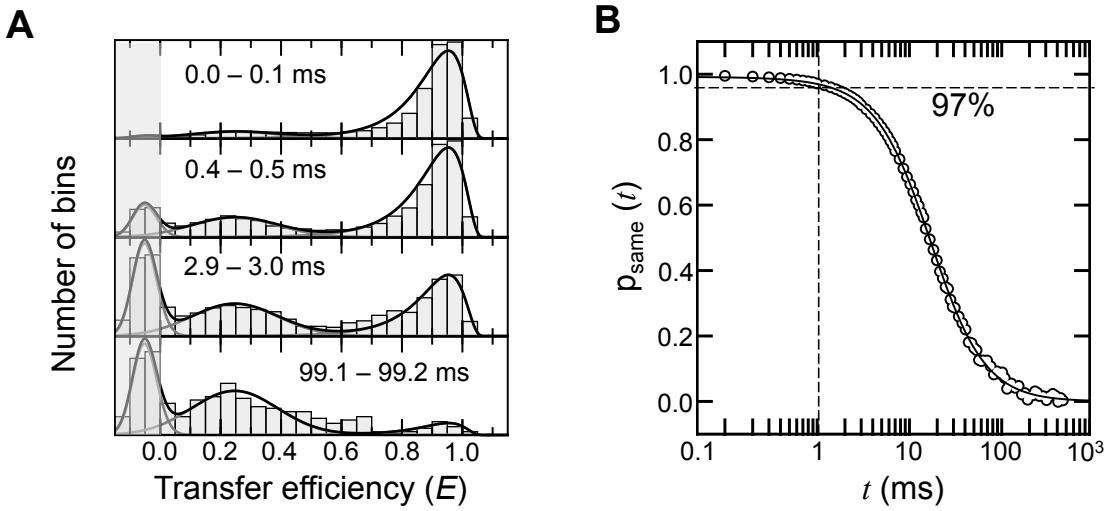

Fig. S1. Open-close kinetics and conformational heterogeneity detected with RASP. (A) Single-molecule recurrence histograms of TbQSOX in the absence of substrate obtained for different delay times (indicated above each histogram) after selecting closed molecules with $E \geq 0.8$. **(B)** Time course of the probability to observe a single molecule twice $p_{same}(t)$ for TbQSOX in the absence of substrate. Dashed lines indicate 1 ms, showing that bins within a ms window have a 97% likelihood to be from the same molecule.

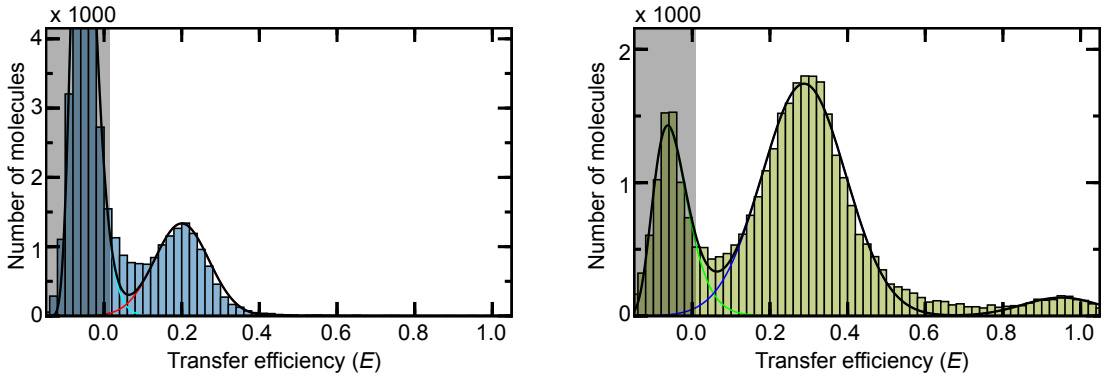

Fig. S2. Transfer efficiency histograms for PEG 5000 (blue) and TbQSOX (green). Experiments were performed at 200 mM NaCl in 20 mM sodium phosphate buffer pH 7.5 including 0.01% Tween 20. Solid lines are superpositions of log-normal (D-only) and Gaussian functions.

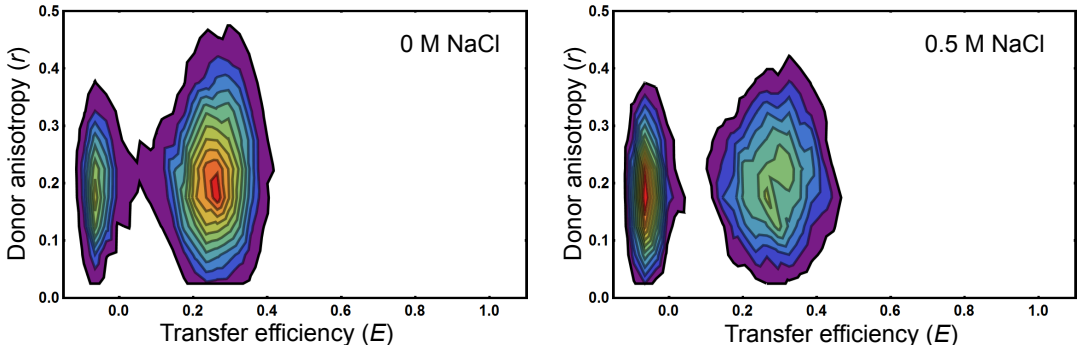

Fig. S3. Donor anisotropies vs. transfer efficiency for TbQSOX in the absence of NaCl (left) and in the presence of 0.5 M NaCl (right). Experiments were performed in 20 mM sodium phosphate buffer pH 7.5 including 0.01% Tween 20.

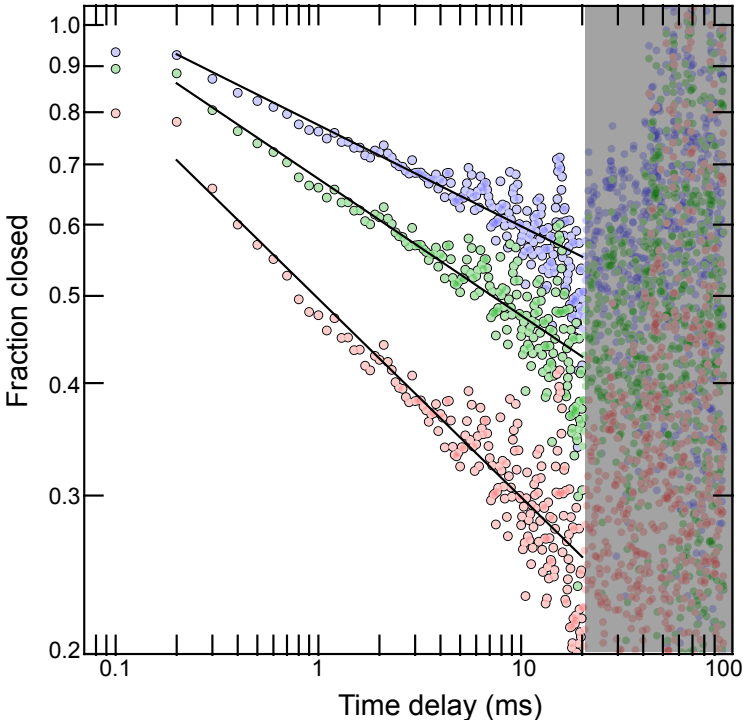

Fig. S4. Recurrence analysis of the data for wt-TbQSOX in the absence of substrate for three different values of the correction factor σ. The kinetics were obtained from the original data using equation 7 using $\sigma = 1.5$ (blue), $\sigma = 1$ (green), and $\sigma = 0.5$ (red). Fits with the equation $p_c(t) = at^{-|\beta|}$ resulted in the exponents

$\beta = 0.11 \pm 0.01$ (blue), $\beta = 0.15 \pm 0.01$ (green), and $\beta = 0.22 \pm 0.01$ (red). Grey area indicates data excluded from the analysis.

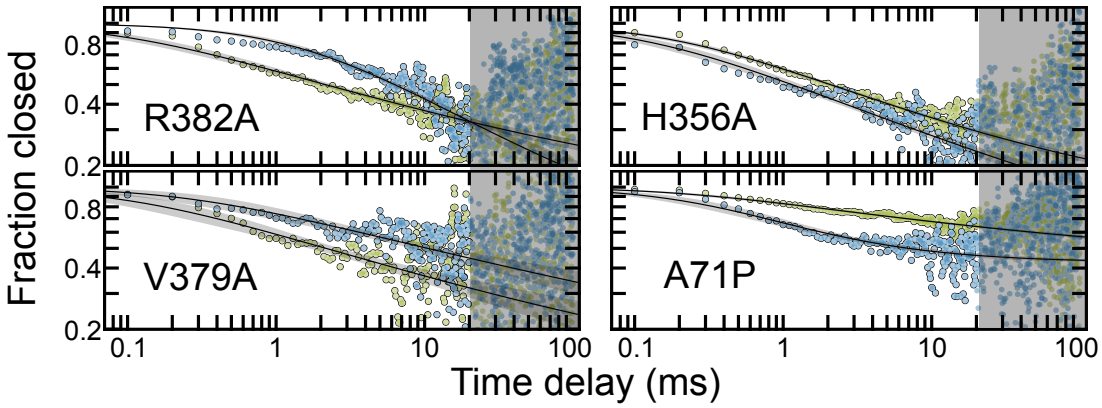

Fig. S5. RASP kinetics of the closed population for the TbQSOX variants in the absence (blue) and presence (green) of 50 mM DTT together with a fit with eq. 2.

References.

1. Grossman I, *et al.* (2015) Single-molecule spectroscopy exposes hidden states in an enzymatic electron relay. *Nature Communications* 6.
2. Schuler B (2007) Application of single molecule Förster resonance energy transfer to protein folding. *Methods Mol Biol* 350:115-138.
3. Hoffmann A, *et al.* (2011) Quantifying heterogeneity and conformational dynamics from single molecule FRET of diffusing molecules: recurrence analysis of single particles (RASP). *Phys Chem Chem Phys* 13(5):1857-1871.
4. Hoffmann A, *et al.* (2007) Mapping protein collapse with single-molecule fluorescence and kinetic synchrotron radiation circular dichroism spectroscopy. *Proc Natl Acad Sci USA* 104(1):105-110.